Three-dimensional grain mapping by x-ray diffraction contrast tomography and the use of Friedel pairs in diffraction data analysis

W. Ludwig,[1,2] P. Reischig,[2] A. King,[2,3] M. Herbig,[1] E. M. Lauridsen,[4] G. Johnson,[2,3] T. J. Marrow,[3] and J. Y. Buffière[1]
[1]*Université de Lyon, INSA-Lyon, MATEIS CNRS UMR 5510, 69621Villeurbanne, France*
[2]*European Synchrotron Radiation Facility, BP220, 38043 Grenoble, France*
[3]*School of Materials, University of Manchester, Manchester, M13 9PL, United Kingdom*
[4]*Risø National Laboratory, Technical University of Denmark, P.O. Box 49, DK-4000 Roskilde, Denmark*

(Received 8 January 2009; accepted 26 February 2009; published online 19 March 2009)

X-ray diffraction contrast tomography (DCT) is a technique for mapping grain shape and orientation in plastically undeformed polycrystals. In this paper, we describe a modified DCT data acquisition strategy which permits the incorporation of an innovative Friedel pair method for analyzing diffraction data. Diffraction spots are acquired during a 360° rotation of the sample and are analyzed in terms of the Friedel pairs ((*hkl*) and ($\overline{hkl}$) reflections, observed 180° apart in rotation). The resulting increase in the accuracy with which the diffraction vectors are determined allows the use of improved algorithms for grain indexing (assigning diffraction spots to the grains from which they arise) and reconstruction. The accuracy of the resulting grain maps is quantified with reference to synchrotron microtomography data for a specimen made from a beta titanium system in which a second phase can be precipitated at grain boundaries, thereby revealing the grain shapes. The simple changes introduced to the DCT methodology are equally applicable to other variants of grain mapping. © *2009 American Institute of Physics.* [DOI: 10.1063/1.3100200]

I. INTRODUCTION

In polycrystalline materials, the orientation, shape, and size of individual grains, or clusters of grains, can have important implications for a range of aspects of the material behavior. In many cases, material behavior at these length scales is poorly understood and there is a need for experimental techniques that allow its study.

X-ray diffraction contrast tomography (DCT) is a technique for the mapping of grain shape and crystal orientation in polycrystalline materials in a nondestructive way. It can be regarded as a variant of the techniques generally known as three-dimensional x-ray microscopy (3DXRD).[1] The basic concepts of DCT have been presented in two previous papers, with examples of the grain maps produced.[2,3]

In this paper, the authors present a number of refinements to the experimental methodology and data analysis techniques previously described and show results illustrating the improvements obtained. The scan range is extended to 360° and the data analyzed in terms of Friedel pairs of diffraction spots, improving accuracy and enabling the use of improved indexing routines. In contrast with previously introduced variants of DCT, which required the visibility of extinction contrast in the transmitted beam, the indexing and reconstruction procedures presented in the current paper are based on the analysis of diffracted beams only. As previously, the attenuation of the simultaneously acquired transmitted beam can be used for reconstruction of the 3D attenuation coefficient distribution in the sample (i.e., absorption contrast microtomography). Quantitative assessment of the grain mapping algorithms was carried out using synchrotron microtomography in a metastable beta titanium alloy in which a second phase was precipitated on the grain boundaries, thereby revealing the 3D grain shape in the tomographic reconstruction. Previous validations of DCT have been limited to two-dimensional (2D) postmortem sections made using electron backscatter diffraction.[3]

II. METHODOLOGY

The principles of DCT and two analysis strategies using the information carried by the direct beam have been described recently.[2,3] The method presented in the current paper introduces the concept of Friedel pair analysis of diffracted beams and combines the advantages of DCT (truly 3D acquisition, single acquisition distance, simultaneously recorded absorption image) and 3D x-ray diffraction (3DXRD) (lesser degree of diffraction spot overlap and better signal to noise for diffracted beams).

A. Acquisition procedure

The experimental apparatus and acquisition procedure are similar to those used for standard synchrotron microtomography (Fig. 1). A parallel, monochromatic beam of synchrotron radiation illuminates the sample, forming an absorption contrast radiograph in the center of the detector, which is placed closely behind the sample. The sample is continuously rotated through 360° around an axis perpendicular to the incident beam and a series of radiographs are recorded integrating over small angular increments (typically 0.05°). In previous versions of the technique, the sample was rotated through 180° only.

During this rotation, grains pass through alignments in which they fulfill the Bragg criteria for diffraction. When this

 © 2009 American Institute of Physics

Downloaded 02 Sep 2011 to 129.49.56.80. Redistribution subject to AIP license or copyright; see http://rsi.aip.org/about/rights_and_permissions

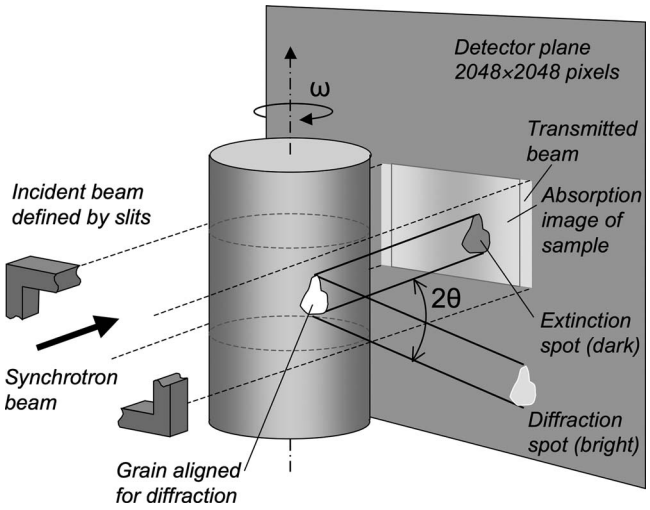

FIG. 1. Schematic of the DCT setup. The detector is placed close behind the sample so that both transmitted and diffracted beams are caught.

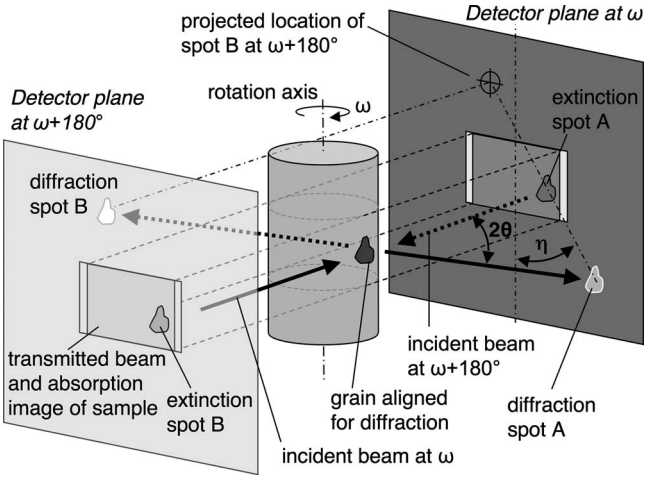

FIG. 2. Representation of a Friedel pair in the reference fixed to the sample. Diffraction spot A appears at ω. Its pair, spot B, is shown on the opposite imaginary detector plane at $\omega+180°$. The diffraction path connecting both passes through the grain of origin.

takes place, intensity is diverted out of the transmitted radiation beam into a diffraction spot. This diffraction spot is recorded on the outer part of the detector and the absorption and extinction information carried by the transmitted beam is recorded in the central part. In general, diffraction spots may spread over several consecutive images and need to be summed and segmented from the background. Information describing the spots (size, location, etc.) are stored in a database. In the absence of significant orientation and strain gradients inside the grain, each diffraction spot can, with suitable processing, be treated as a parallel projection of the grain from which it arises.

B. Data analysis based on Friedel pairs

Friedel pairs are the key to both the efficiency and the accuracy of the novel data processing route presented here. During the rotation of the sample, the angle between a given crystal plane of a grain and the incident beam varies sinusoidally between zero and some maximum value. In a full 360° rotation this angle coincides with the Bragg angle a maximum of four times (provided the angle between the rotation axis and the plane normal is bigger than the Bragg angle). Thus, each set of lattice planes can give rise to a maximum of four diffraction spots, which make up two pairs, each separated by a 180° rotation of the sample. Such pairs are called Friedel pairs and they are the Bragg reflections from the (hkl) and $(\overline{hkl})$ lattice planes of the grain. Relative to the sample, the pair of scattering vectors and the associated diffracted beams are parallel but have the opposite sign.

To understand the advantage of the Friedel pair geometry, it is useful to consider a reference system, in which the sample is fixed, and the synchrotron beam and detector rotate relative to the sample (Fig. 2). It can be seen that the two diffracted beams forming the diffraction spots of the Friedel pair are parallel and coincident, sharing a common point of origin in the diffracting grain. Thus, the two spot positions define the path of diffracted beam and it is possible to calculate the diffraction angles associated with the scattering event without reference to the position of the grain in the sample. Furthermore, it is clear that the grain must lie on the diffracted beam path. The scattering vector (diffracting plane normal) and the $\{hkl\}$ lattice plane type for the diffraction event can be found from the diffraction angles. All of this information, together with shape, size, and other properties of the diffraction spots, can be used to improve the indexing process, in which diffraction spots are sorted according to the grain from which they arise.

By using the centers of mass of the two spots, the diffraction angles can be calculated with high accuracy. In the absence of orientation and strain gradients, the paired diffraction spots are mirror images of each other and therefore contain identical shape information. An additional benefit is that in calculating the diffraction angle using two diffraction spots, the distance between the spots along the direct beam is effectively twice the sample-detector distance thereby improving the angular resolution. By optimizing the experimental conditions, it is possible to achieve sufficient accuracy in the determination of the diffraction angles to measure elastic lattice strains on a grain-by-grain basis in an *in situ* loaded sample. The details of this measurement and the analysis techniques used are described elsewhere.[4]

Errors in the determination of each scattering vector can be estimated as the difference between the vectors calculated from the two Friedel pairs, provided that both have been detected. Considering them as independent observations is reasonable, since after correction for systematic errors (detector distortions, sample drifts, etc.), the most significant error in the scattering vectors originates from the random error in determining the center of mass of the diffraction spots.

C. Finding Friedel pairs

To exploit the available information, it is necessary to identify the diffraction spot pairs in images separated by a 180° rotation. As in the previous procedure, after initial image processing operations, diffraction spots are segmented from the images, and data describing their shape, size, position, etc., are stored in a database. If the lattice type and

Downloaded 02 Sep 2011 to 129.49.56.80. Redistribution subject to AIP license or copyright; see http://rsi.aip.org/about/rights_and_permissions

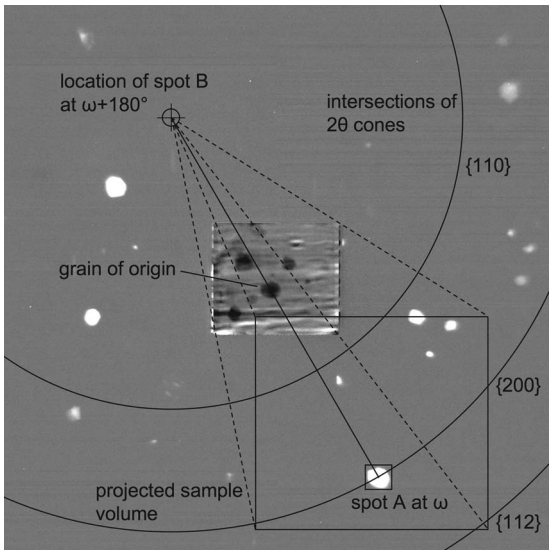

FIG. 3. Geometric and crystallographic criteria for finding Friedel pairs. Spot A, the corresponding pair of spot B is found in the images at a rotational offset of about 180° (preprocessed image belonging to spot A is shown). The search area is restricted to the projected sample volume (the square) and to narrow circular bands along the intersections of the detector plane and cones originating from spot B with varying 2θ opening angles.

lattice parameters of the sample and the energy of the radiation used are known, it is possible to calculate the allowed diffraction angles ($\theta_{\{hkl\}}$). Using the same fixed sample coordinate system described above, the diffraction cones (with $2\theta_{\{hkl\}}$ opening angles) corresponding to these angles can be drawn based on the first diffraction spot. These cones intersect the 180° offset detector as circles and the second diffraction spot of the pair must lie on one of these (Fig. 3). It is also known that the grain must lie in the volume of the sample illuminated by the direct beam. This imposes the further constraint that the second diffraction spot must lie within the region formed by projecting this volume, from the position of the first spot, on to the 180° detector. The size, shape, and intensity of the paired spots should also be similar. By using these criteria with suitably selected tolerances, pairs of spots can be found easily and reliably. It is not possible to find the pairs of all diffraction spots, because in some cases one of the pair will fall outside the detector area, or may overlap with another diffraction spot or the direct beam. As will be explained later, it is not necessary that all spots be paired, as single diffraction spots can be dealt with later. The number of spot pairs found in a data set comprising of 10^2–10^3 grains (with cubic symmetry) is typically in the order of 10^3–10^4.

If the sample crystallography is not known, it is still possible to identify pairs of spots that are well matched using the other criteria. In simple cases this diffraction data could be used to determine the crystallography of an unknown material.

D. Indexing from Friedel pairs

A robust indexing procedure ("indexter") has been developed to exploit the information available from the diffraction spot pairs. This uses all spatial and crystallographic criteria simultaneously to form consistent sets, in a reliable and computationally efficient manner, of diffraction spot pairs belonging to the same grain. The algorithm consists of an iteration over three main processes which are executed sequentially. This is shown schematically in Fig. 4.

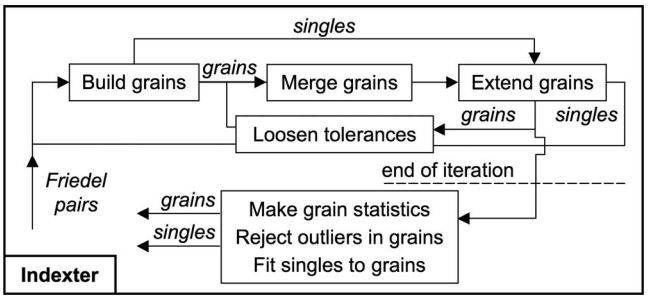

FIG. 4. Flow chart of the iterative indexing procedure

Build grains: The base of the algorithm finds noncomplete groups of Friedel pairs that originate from the same grains.

First an arbitrary Friedel pair is chosen, and all the others are checked for consistency with it, by considering the spot properties (areas, sizes, etc.), the crystallographic consistency of the angles between the diffracting plane normals, and the distances between the diffracted beams in the sample coordinate system.

Second, a systematic search is carried out among those pairs that passed the first selection. If a mutually consistent subset is found containing a minimum number of pairs (typically this parameters is chosen to be in the range of 5–10), it is stored as a grain. Those pairs from the first selection that do not disrupt this consistency are added to the grain. If no grain is found, the initially selected Friedel pair is output as a "single" (a pair not assigned to a grain). Finally, other grains are sought by the repetition of this procedure excluding singles and those pairs that have already been associated with a grain.

Merge grains: If there are grain sets that represent two overlapping volumes with the same orientation, they actually belong to the same grain and will be merged together. Once a new grain is created by merging, statistics of positional and angular accuracy are calculated and the tolerances used in the extend grains procedure for that grain are updated accordingly.

Extend grains: Pairs that were left unassigned by build grains but that are found to be consistent with one of the merged grains are incorporated.

The loop is repeated several times with decreasingly strict tolerances, until tolerance limits fixed by the operator are reached. This gives robust indexing by minimizing the chance of wrong assignments in the first loops, while ensuring that most of the pairs are indexed by the last iterations.

After the final iteration, detailed statistics of the variations in diffraction spot properties and discrepancies in the fit of the diffraction data to the orientation and location of each grain are collected and stored for later analysis if required. Based on the relatively high number of pairs per grain, outliers can be rejected on a purely statistical basis by determining whether they fit in the observed distributions. Similarly, a

Downloaded 02 Sep 2011 to 129.49.56.80. Redistribution subject to AIP license or copyright; see http://rsi.aip.org/about/rights_and_permissions

measure of the goodness of fit of all remaining unassigned pairs to every existing grain set can be determined. These pairs are added to the grain set they fit the best, provided the goodness of fit is satisfactory.

Once the grain positions and orientations have been identified, the locations of all other diffraction spots belonging to each grain can be predicted and, hence, other unpaired, diffraction spots added to the sets. As previously,[3] the orientation of each grain is inferred from the point in the fundamental zone of Rodriguez space,[5] where all projection lines for pole figure inversion of the corresponding grain cross (each of the observed scattering vectors defines one of these projection lines in Rodriguez's space).

E. Shape reconstruction by algebraic reconstruction techniques

After indexing, the 3D shape and position reconstruction is performed independently for each grain by means of algebraic reconstruction techniques[6] (ARTs), or any other suitable algorithm for tomographic data with limited numbers of projections. For this the summed diffraction spots are normalized and treated as parallel projections of the grain. Using the diffraction spots has several advantages over the extinction spots previously used.[2,3] They are much less affected by spot overlap, as they are spread over a larger area of the detector. Because diffraction spots are recorded as a bright spot on a dark background, whereas the extinction spots are recorded as missing intensity in the direct beam, the diffraction spots have better contrast and are less affected by noise. The improved accuracy of the diffraction vectors calculated from the Friedel pairs allows the use of 3D (oblique angle) ART reconstruction. Alternatively, grain reconstruction can also be performed using a more widely available 2D (parallel beam) ART reconstruction algorithm by placing the diffraction spot projections at the position where the corresponding extinction spot would be observed. The shape of the projection is corrected by allowing for the true omega angle of the projection and the shear distortion resulting from the nonnormal angle of incidence of the diffracted beams on the detector.

F. Optional postprocessing of the grain map

By placing the individual grain reconstructions at their correct positions within the sample volume, the final grain map is assembled. Postprocessing operations are used to resolve cases where a voxel is not assigned to a grain, or is assigned to more than one grain. If these ambiguous voxels are left unlabelled one obtains a grain map that is not completely space filling. An approximation of the real, space filling grain map can be obtained from this initial map by a 3D morphological dilation process of the grains into the unlabeled voxels until all the unclaimed or disputed voxels have been assigned.[7] Grain labels are not allowed to grow into other grains, or grow beyond the sample volume as found from the absorption reconstruction.

G. Implementation

The data analysis procedure outlined in the previous paragraphs has been implemented using the MATLAB® programming environment. Most of the sequential processing steps can be performed in parallel on a subset of the data. The use of a central database for storage of the metadata and parallel processing of computing jobs on a cluster of machines helps reduce the processing time, which roughly scales with the number of grains or diffraction spots. Using a computing cluster of 50 nodes, a data set comprising of 1000 grains can currently be analyzed in one day. This time could further be reduced by optimization of the code and the possible use of hardware accelerators for computational intense tasks.

III. EXPERIMENTAL VALIDATION

To validate the grain maps produced by the data collection and processing route described in Sec. II, a DCT data set was acquired from a specimen in which it was possible to decorate the grain boundaries by precipitation of a second phase, and thereby image the 3D grain shapes directly using propagation based phase contrast tomography (PCT).[8] Since precipitation may entail an increase of the local effective misorientation inside grains, the acquisition of the DCT scan was performed in the initial state before heat treatment. The reconstruction of the DCT grain map was performed without input from the PCT data set. The extraction of the grain boundary network from the PCT data set was performed using the DCT map as a seed map for the watershed segmentation process.

A. Materials and methods

The metastable β-titanium (bcc) alloy Timet 21S (Ti–15Mo–3Nb–3Al wt %) was selected as a suitable material. It provides the possibility of directly imaging the grain shapes in PCT through the precipitation of a second phase on the grain boundaries.[9] It is possible to produce microstructures consisting of large equiaxed beta grains (bcc) with low mosaicity (i.e., low subgrain misorientation) and its density and atomic numbers are low enough to give only limited absorption at the acquisition energy, thus forming diffraction spots that appear clear and undistorted. Before the DCT acquisition, the 0.6 mm diameter sample was annealed in vacuum for 2 h at 830 °C. The heat treatment allowed recovery of any residual stresses or plastic deformation introduced during sample manufacture and increased the average beta grain size to 55 μm. This was calculated subsequently from the 777 complete grains in the DCT grain map.

The DCT data acquisition was performed at beamline ID11 of the ESRF using a FReLoN charge coupled device camera[10] with a transparent luminescent screen and optics giving an effective pixel size of 1.4 μm. The x-ray energy was 40 keV and 7200 images were recorded during a 360° rotation of the sample, with a distance between sample and detector of 4 mm. The overall scan acquisition time using a Si (111) double crystal monochromator in Bragg–Bragg reflection ($\Delta\lambda/\lambda \sim 10^{-4}$) was 20 h (more recently, the overall acquisition time could be reduced to less than 2 h using a

Downloaded 02 Sep 2011 to 129.49.56.80. Redistribution subject to AIP license or copyright; see http://rsi.aip.org/about/rights_and_permissions

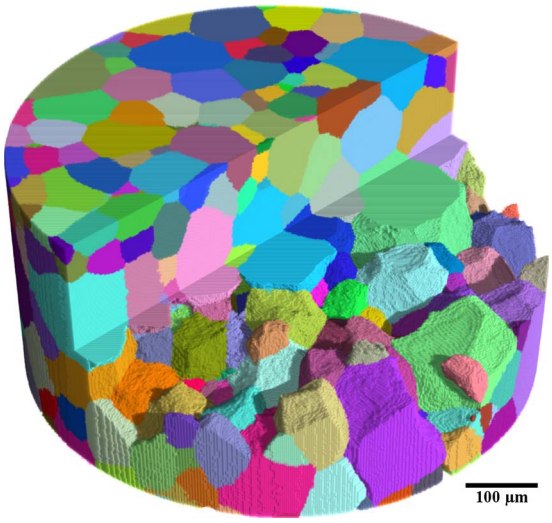

FIG. 5. (Color online) Rendition of the 3D grain structure in a cylindrical beta-Ti specimen containing 1008 grains, as obtained by the DCT processing route described in this paper.

monochromator with a relative bandwidth of 10^{-3}). The grain map was reconstructed using the data processing route described in this paper. A 3D rendered view of the resulting map is shown in Fig. 5.

A second heat treatment of 24 h at 790 °C was used to produce a thin film of grain boundary α (hcp) precipitates. The alpha phase is enriched with Al, while the beta phase is enriched in Mo and Nb, as verified by energy dispersive x-ray spectroscopy. This leads to a detectable difference in electron density in PCT. A tomographic reconstruction of the heat treated sample was produced from data acquired at beamline ID19, ESRF. 1000 images were acquired at a pixel size of 0.56 μm, using an energy of 40 keV and a sample to detector distance of 150 mm. (Fig. 6)

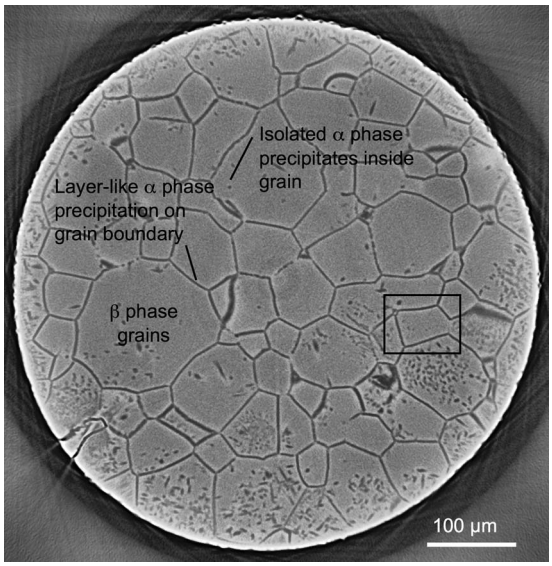

FIG. 6. Cross section through the PCT reconstruction. The α-phase appears dark. It precipitated during a heat treatment for 24 h at 790 °C performed after acquisition of the DCT scan. The rectangle marks the area on which the image processing for the completion of grain boundaries is illustrated (Fig. 7).

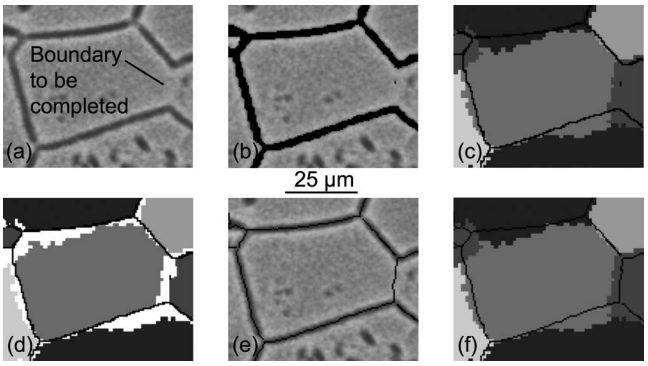

FIG. 7. Image processing steps for the completion of the grain boundaries not visible in PCT. (a) Shows the original PCT image after median filtering and contrast enhancement. One grain boundary is not visible and shall be completed. First, the grain boundaries are labeled semiautomatically as far as visible (b). The overlay of the slimmed labeled grain boundaries with the DCT image (c) shows that some DCT grains extend over the grain boundaries. Those parts have to be removed (d) before the DCT image can be used as marker image for the watershed algorithm. (e) The missing grain boundary was completed. Note that the originally labeled grain boundaries remain unaffected by the algorithm. The accuracy of DCT was determined from the completed network of grain boundaries and the DCT data (f). (The average error for the grain shown in this figure is 4.1 voxels or 2.3 μm).

B. Image processing and segmentation

The PCT data set showing the grain boundary precipitation can be used as a reference against which to assess the accuracy of grain shapes in the DCT grain map. However, it does not produce a perfect grain boundary map, because during the second heat treatment, a small fraction of grain boundaries are not decorated with the precipitated phase, and a certain amount of undesirable intragranular precipitation occurs. These features must be corrected before it is possible to extract the complete boundary network required for automated, quantitative comparisons. The following processing route, incorporating some prior knowledge from the DCT map, has been developed to determine an accurate grain map from the PCT data. All measurements and image processing steps were done using MATLAB® and the image processing toolbox DIPIMAGE.[11]

Prior to processing, the DCT volume was scaled (oversampling by a factor of 2.5) to give the same effective voxel size of the PCT volume and the two data sets aligned.

Initial segmentation: The PCT data was denoised using a median filter and its contrast enhanced using contrast-limited adaptive histogram equalization. A region growth algorithm was performed to segment the grain boundaries as regions of interest (ROIs). After a morphological closing of the ROI, very small, isolated regions (mostly intragranular precipitates) were excluded by applying a size filter. Intragranular precipitates still erroneously assigned to the ROI were excluded manually. Decorated grain boundaries not yet belonging to the ROI were included manually.

Restoration of boundaries: The resulting network of boundaries still contained some gaps due to the presence of nondecorated boundaries. As illustrated in Fig. 7, those gaps were filled with the help of a 3D watershed algorithm, using the DCT grain map as markers to avoid oversegmentation. The network of grain boundaries from the PCT data and the DCT grain map had to be modified in order to serve as a

Downloaded 02 Sep 2011 to 129.49.56.80. Redistribution subject to AIP license or copyright; see http://rsi.aip.org/about/rights_and_permissions

good ridgeline and marker map, respectively. The PCT network of grain boundaries was reduced in thickness to give accurate final grain outlines. The markers (derived from the DCT map after postprocessing) should be as big as possible to attain good results, but must not overlap with the network of grain boundaries. Due to the remaining inaccuracy of the DCT map, the latter condition is not fulfilled and optimization of the marker map was done by performing the watershed algorithm without markers on the slimmed network of grain boundaries from the PCT data, yielding a closed but slightly incorrect network of grain boundaries due to oversegmentation. This network was applied to the DCT grain map, thereby dividing DCT grains that overlapped with the network of grain boundaries. The marker map was created out of the biggest subvolume of each DCT grain. This marker map was used to obtain a final grain boundary map. Note that it is the original ridgeline map that determines the boundary network shape and the marker map only determines how the nonvisible grain boundaries are restored. Therefore it is valid to the resultant boundary map to be used to assess the DCT map.

The validation of the DCT grain map by this method relies on the precision of the grain boundary network segmented from the PCT. Errors in this segmentation will influence the result of this validation. Even when considering the errors from the acquisition and reconstruction of the PCT volume to be negligible, the errors due to image processing have to be discussed. During the alignment and scaling of the volume some aliasing errors are introduced due to the voxel nature of the data, but the effect of these errors should be small. Error sources of probably higher impact are the nondecorated grain boundaries, which were not segmented due to the absence of precipitates, and the grain boundaries close to the surface that were hardly visible because their contrast was superimposed by the strong phase contrast between sample and surrounding air. These invisible boundaries are restored by the watershed algorithm and represent less than 5% of the total boundary area. Therefore errors introduced by this method are not expected to have a significant effect on the final results.

IV. RESULTS

A. Diffraction data

The accuracy with which diffraction data are observed can be assessed using the redundant measurements of the scattering vectors from which two Friedel pairs are observed. For the current data set the mean angular deviation between such pairs is 0.051°. The same measure can also be determined for the same data set processed using the previous methodology.[3] In this case a maximum of four observations of each scattering vector is possible (one for each diffraction spot) and the mean angular deviation is found to be 0.255°. Thus the introduction of the Friedel pair analysis gives five times improvement. The mean angular deviation in the Bragg angle was estimated to be 0.0042° and 0.043° in η.

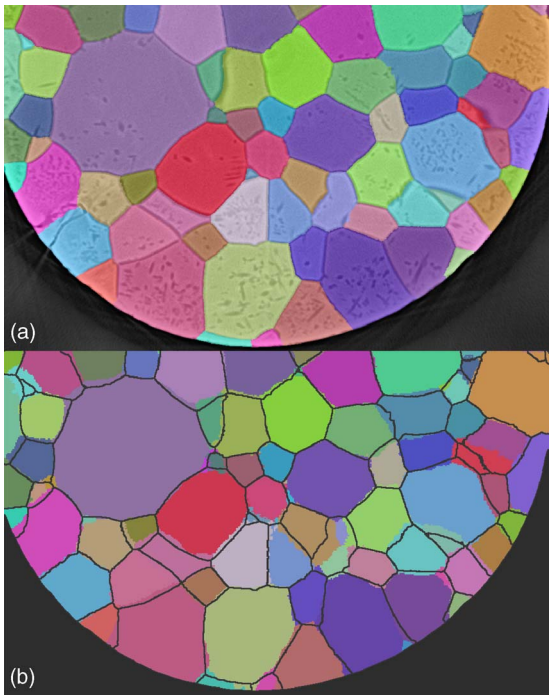

FIG. 8. (Color online) Cross sections through the (a) PCT and (b) DCT reconstructions showing the corresponding segmented grains in identical color. Grain boundaries from the PCT volume are also shown in black for comparison in (b).

B. Comparison of PCT-DCT

All grains visible in the PCT data are also found in the DCT map and the grain shapes and size appear to be very similar in all cases. Figure 8 shows a section through the DCT grain map with the boundaries segmented from the PCT data as an overlay. The accuracy of the 3D grain shapes determined by DCT was quantified by comparing the PCT and DCT grain maps on a grain-by-grain basis. First, a 3D Euclidean distance transform was applied on the grain outline of a PCT grain. Then, this volume was multiplied with the outline of the same grain from the DCT map The values of this intersection represent the closest distance between the two outlines, or alternatively the error of DCT. The average error in the DCT grain outlines was found to be 2.6 μm (4.7 voxels in the PCT map, corresponding to 1.9 voxels in the DCT grain map) (Fig. 9).

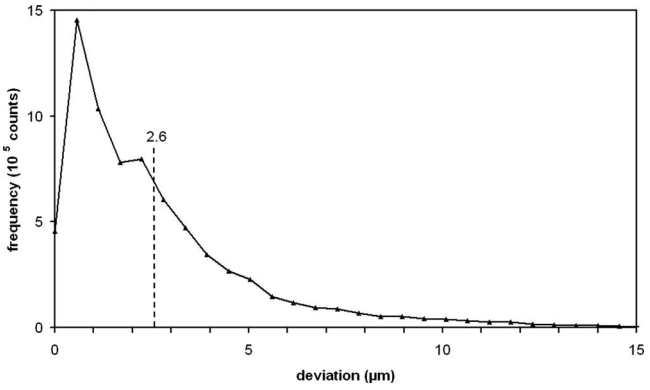

FIG. 9. Histogram of the deviation in the grain boundary locations between the PCT and DCT data.

Downloaded 02 Sep 2011 to 129.49.56.80. Redistribution subject to AIP license or copyright; see http://rsi.aip.org/about/rights_and_permissions

V. DISCUSSION

A. Sample requirements for DCT

The simultaneous, extended beam illumination of a large number of grains requires some conditions in terms of deformation state, texture, and grain size of the material to be fulfilled to make it amenable for this type of characterization:

- The presence of orientation gradients inside a grain leads to the violation of the parallel projection approximation and may result in distortion and breakup of diffraction spots. The inverse reconstruction procedure outlined in the present paper cannot correctly handle such cases. For this reason DCT works best for microstructures exhibiting only limited levels of intragranular orientation spread (typically below 1°).
- Despite the high angular resolution provided by the DCT indexing approach it can (for similar reasons to the ones mentioned in the previous paragraph) be problematic to accurately reconstruct grains that are divided into subgrains by small angle grain boundaries with low misorientation values ($<2°$).
- The indexing procedure presented has proven to be robust and applicable to sample volumes containing up to a few thousands of grains. The typical size of the illuminated area (500×500 pixels on a 2048×2048 pixels detector) and the requirement to have sufficient spatial sampling of the diffraction spots for 3D shape reconstruction ($>20\times20$ pixels) result in some typical boundary conditions concerning maximum sample size and minimum grain size (both expressed in terms of detector pixels). Consequently, a large range of physical sample and grain sizes can be investigated by appropriate choice of beam energy and pixel size of the detector system (energies between 15 and 50 keV and resolutions between and 1 and 20 μm have been explored so far for different material systems).

B. Comparison to 3DXRD

By indexing grains directly from diffraction spot data, the new methodology presented represents a partial convergence between DCT and 3DXRD (Ref. 1) from which it was originally derived. However, it retains some distinctive features, namely, that a 2D box (rather than a 1D line focused) beam is used to illuminate the sample, and that the absorption images are acquired simultaneously with the diffraction spots, allowing a reconstruction of the absorption contrast microstructure of the sample. This has significant benefits in speed of data collection and analysis by combined techniques.

The Friedel pair analysis used to determine the diffracted beam paths is similar to the 3DXRD concept in which the detector is moved and the diffraction spot positions recorded at a series of distances from the sample.[12] In that case the diffraction angles can then be calculated using the shift in spot position between the different detector distances. In the Friedel pair method, the detector is not moved, but effectively the diffraction spot is recorded at two distances ($\pm$ the sample-detector distance). This is advantageous because a single optimized sample detector distance can be used, the effective distance between the two detector positions is usually larger and alignment problems resulting from nonreproducible movements of the detector are avoided.

C. Comparison to DCT-180° methodology

The described methodology for 360° rotation has significant advantages compared to the previously described 180° DCT methodology.[2,3] By allowing indexing directly from the diffraction spots, without reference to the extinction spots, the requirements of very low grain mosaicity and only limited extinction spot overlap are significantly relaxed. However, in those materials with suitable microstructures, the extinction spots are still available and can still be used as additional grain projections. The need for a computationally intensive image correlation step to find the extinction spot corresponding to a diffraction spot is no longer necessary once the grain center is known from the indexing step. The diffraction data measured using Friedel pairs are also significantly more accurate than can be determined in the 180° case.

The methodology described maintains the use of small angular increments of sample rotation. This was initially required to achieve maximum contrast in the extinction spots and to minimize extinction spot overlap. However, it also has other benefits for the diffraction spot based analysis. By reducing the number of diffraction spots in each image, diffraction spot overlaps are also reduced and the chance of erroneous matches when determining Friedel pairs is reduced. In addition, the improved resolution of the diffraction event in omega (sample rotation) affects the precision with which the scattering vector can be determined. This is an important consideration if elastic strain is to be determined.

D. Comparison to acquisition by a far-field detector

The accuracy of determination of the diffraction angles can be improved in all cases by using a detector with a larger pixel size, located far from the sample. In this case angular sensitivity is improved at the expense of spatial resolution (sensitivity to grain position). The described DCT methodology has the advantage of combining good angular and spatial resolution for reliable indexing. The concept of Friedel pairs can of course be applied to far-field diffraction data to achieve the best possible angular sensitivity.

E. Comparison to polychromatic microdiffraction methods

Polychromatic x-ray diffraction in combination with differential aperture x-ray microscopy[13,14] is a powerful tool for probing the 3D grain structure in polycrystalline materials at the submicrometer length scale. Since the 3D scanning procedure isolates the signal from small volume elements, this method can be applied to plastically deformed specimen and provides access to local orientation and deviatoric components of the elastic strain tensor. However, the requirement to scan the sample in three dimensions implies some limitations

Downloaded 02 Sep 2011 to 129.49.56.80. Redistribution subject to AIP license or copyright; see http://rsi.aip.org/about/rights_and_permissions

in time resolution and sample volume that can be analyzed with this technique (typically a few tens to hundreds of micrometers).

DCT, on the other hand, can cover length scales between a couple of hundred micrometers up to several millimeters and works best for plastically undeformed grain microstructures in which each grain can be described by an average crystallographic orientation. The illumination of a sample volume containing thousands of grains enables fast measurement of a statistically relevant number of grains and the possibility of direct combination with high resolution x-ray tomography makes this technique highly complementary to polychromatic microdiffraction.

F. Sensitivity to elastic strain

The analysis of redundant pairs of diffraction spots indicates accuracy in the determination if the Bragg angle is $0.004°$ or 7.3×10^{-5} rad. This value suggests that it must be possible to measure (average) elastic strains from individual reflections with a precision of order of $\Delta\varepsilon=\Delta\theta\cot(\theta)\approx4\times10^{-4}$ (from the derivation of Bragg's law). This conservative estimate is based on a Bragg angle θ of $10°$ and assumes that systematic errors arising from spatial distortion, mechanical drifts of the instrument, and uncertainties in the alignment can be determined and reduced to comparable levels. Further improvement in accuracy and access to the full strain tensor on a grain by grain basis may be expected using a fitting routine that combines the multiple measurements that are available for each grain.

G. Alternative reconstruction approaches

As opposed to the inverse reconstruction approach presented in the current paper, one may envisage reconstruction of grain maps by forward simulation approaches. In this case one seeks (by assigning orientations to voxels in sample space) the configuration that minimizes the difference between experimentally observed and simulated diffraction patterns.[15,16] Such algorithms can account for local variations in orientation inside grains and may overcome the current restriction to low levels of orientation spread. Some encouraging results have been obtained for 2D (line focus illumination of one sample cross section) simulated data of deformed specimen[16] and first 3D maps for an undeformed specimen have been obtained from stacking of 2D data.[17]

It can be expected that the combination of DCT with such minimization procedures will further improve the accuracy of grain maps provided by DCT. For the case of undeformed specimen, the current postprocessing (3D morphological dilation) may be replaced by testing, for each of the ambiguous voxels, the goodness of fit between simulated and measured diffraction patterns, when assigning the orientation of one of the neighboring grains.

H. Alternative acquisition geometries

One may consider two alternative acquisition procedures for accommodation of extended, sheetlike sample geometries: (i) reduction of the omega scanning range to the symmetric interval $\pm[\Delta,180\text{-}\Delta]$ and (ii) scanning with an inclined rotation axis, equivalent to laminography[18,19] acquisition geometry. However, in both cases some additional complications arise. For instance, one has to deal with a larger number of spots (possible overlaps) and reduced quality of reconstruction (limited angular interval) in the first case and with the absence of Friedel pairs in the second configuration. In both cases an optimized design of the detector head is required in order to fulfill the proximity constraint (distance between rotation axis and detector comparable to the detector field of view).

VI. CONCLUSIONS

The DCT methodology presented represents significant progress over previous versions.[2,3] By determining the diffraction data more accurately, the indexing step of the processing is made more reliable and can be more readily automated than previously. Improved grain mapping and diffraction data, and an extended range of materials to which it may be applied, make DCT a more useful tool that may be applied to scientific problems.[19] The improved determination of diffraction angles using Friedel pairs opens the possibility of achieving sensitivity to elastic strain at the level of individual grains. The concept of using Friedel pairs to determine diffraction data is equally applicable to other variants of polycrystal indexing and 3D grain mapping.

ACKNOWLEDGMENTS

We would like to express our gratitude to ESRF staff members from the experiments, computing, and engineering division, for their support and their contribution to the successful implementation of DCT. We thank Richard Fonda for providing the material and sharing his experience in heat treatment, as well as Jose Baruchel and Sybrand van der Zwaag for their support of the work. W.L. and E.M.L. acknowledge the Danish National Research Foundation for supporting the Center for Fundamental Research: Metal Structures in 4D, within which part of this work was performed and E.M.L furthermore acknowledges the support jointly sponsored by the Office of Naval Research and DARPA as part of the Dynamic 3-D Digital Structure Program (Grant No. N00015-05-1-0510). A.K. and G.J. wish to acknowledge funding received from the UK Engineering and Physical Sciences Research Council (Crack Nucleation and Short Crack Behavior by Non-destructive *In-situ* Observation, Grant No. EP/C002946).

[1] H. F. Poulsen, *Three-Dimensional X-ray Diffraction Microscopy. Mapping Polycrystals and their Dynamics. Springer Tracts in Modern Physics* (Springer, Berlin, 2004).
[2] W. Ludwig, S. Schmidt, E. M. Lauridsen, and H. F. Poulsen, J. Appl. Crystallogr. **41**, 302 (2008).
[3] G. Johnson, A. King, M. Gonclaves Honnicke, J. Marrow, and W. Ludwig, J. Appl. Crystallogr. **41**, 310 (2008).
[4] P. Reischig, "Determination of elastic strain tensors of individual grains in polycrystals by means of diffraction contrast tomography," M.S. thesis, Delft University of Technology, 2008.
[5] A. Heinz and P. Neumann, Acta Crystallogr., Sect. A: Found. Crystallogr. **47**, 780 (1991).
[6] A. C. Kak and M. Slaney, *Principles of Computerized Imaging* (IEEE, 1988).

Downloaded 02 Sep 2011 to 129.49.56.80. Redistribution subject to AIP license or copyright; see http://rsi.aip.org/about/rights_and_permissions

[7] For a more detailed description of the postprocessing operations the reader is referred to Ref. 3.
[8] P. Cloetens, M. Pateyron-Salomé, J. Y. Buffière, G. Peix, J. Baruchel, F. Peyrin, and M. Schlenker, J. Appl. Phys. **81**, 5878 (1997).
[9] S. R. Dey, E. M. Lauridsen, W. Ludwig, D. J. Rowenhorst, and R. W. Fonda, in *Proceedings of Ti-2007 Science and Technology*, edited by M. Ninomi, S. Akiyama, M. Ikeda, M. Hagiwara, and K. Maruyama (The Japan Institute of Metals, Sendai, Japan, 2007), p. 467–470.
[10] J. C. Labiche, O. Mathon, S. Pascarelli, M. A. Newton, G. G. Ferre, C. Curfs, G. Vaughan, A. Homs, and D. F. Carreiras, Rev. Sci. Instrum. **78**, 091301 (2007).
[11] See www.diplib.org for image processing toolbox for MATLAB® (Tu Delft).
[12] E. M. Lauridsen, S. Schmidt, R. M. Suter, and H. F. Poulsen, J. Appl. Crystallogr. **34**, 744 (2001).
[13] B. C. Larson, W. Yang, G. E. Ice, J. D. Budai, and J. Z. Tischler, Nature (London) **415**, 887 (2002).
[14] G. E. Ice, B. C. Larsen, W. Yang, J. D. Budai, J. W. L. Pang, R. I. Barabash, and W. Lui, J. Synchrotron Radiat. **12**, 155 (2005).
[15] R. M. Suter, D. Hennessy, C. Xiao, and U. Lienert, Rev. Sci. Instrum. **77**, 123905 (2006).
[16] L. Rodek, H. F. Poulsen, E. Knudsen, and G. T. Herman, J. Appl. Crystallogr. **40**, 313 (2007).
[17] S. Schmidt, U. L. Olsen, H. F. Poulsen, H. O. Sørensen, E. M. Lauridsen, L. Margulies, C. Maurice, and D. Juul Jensen, Scr. Mater. **59**, 491 (2008).
[18] L. Helfen, T. Baumbach, P. Mikulik, D. Kiel, P. Pernot, P. Cloetens, and J. Baruchel, Appl. Phys. Lett. **86**, 071915 (2005).
[19] A. King, G. Johnson, D. Engelberg, W. Ludwig, and J. Marrow, Science **321**, 382 (2008).

Downloaded 02 Sep 2011 to 129.49.56.80. Redistribution subject to AIP license or copyright; see http://rsi.aip.org/about/rights_and_permissions